Agenzia nazionale per le nuove tecnologie,
l'energia e lo sviluppo economico sostenibile

MINISTERO DELLO SVILUPPO ECONOMICO

Ricerca di Sistema elettrico

Simulazione Diretta di una Fiamma Premiscelata Metano/Idrogeno/Aria

D. Cecere, E. Giacomazzi, F.R. Picchia, N. Arcidiacono

Report RdS/PAR2013/270

SIMULAZIONE DIRETTA DI UNA FIAMMA PREMISCELATA METANO/IDROGENO/ARIA

D. Cecere, E. Giacomazzi, F.R. Picchia, N. Arcidiacono, (ENEA, UTTEI-COMSO)

Settembre 2014

Report Ricerca di Sistema Elettrico
Accordo di Programma Ministero dello Sviluppo Economico – ENEA
Piano Annuale di Realizzazione 2013
Area: Produzione di energia elettrica e protezione dell'ambiente
Progetto: B.2 - Cattura e sequestro della CO2 prodotta dall'utilizzo di combustibili fossili
Obiettivo: Parte A - b - Tecnologie per l'ottimizzazione dei processi di combustione
Task b.1 - Metodologie numeriche avanzate per la simulazione dei processi di combustione e la progettazione di componenti
Responsabile del Progetto: Stefano Giammartini, ENEA

Indice

Sommario

Negli ultimi anni, grazie all'avvento di computer ad alte prestazioni e avanzati algoritmi numerici, la simulazione numerica diretta (DNS) della combustione é emersa come un valido strumento di ricerca insieme alla sperimentazione. Per comprendere l'influenza della turbolenza sulla struttura della fiamma, in questo lavoro si effettuata una DNS tridimensionale di una fiamma premiscelata magra CH_4/H_2-Aria. Il regime di fiamma premiscelata é quello del Thin Reaction Zone. Si é utilizzato uno schema cinetico dettagliato per la chimica del Metano-Aria costituito da 22 specie e 73 reazioni elementari. Inoltre per la discretizzazione spaziale delle equazioni é stata adottato uno schema al sesto ordine compatto sviluppato in ENEA per flussi comprimibili e griglie staggerate. Sono state calcolate in fase di post processing le velocit di spostamento del fronte di fiamma (individuato da isosuperfici di variabile di progresso) in funzione delle curvature e dello strain-rate e le probability density function (PDF) di queste grandezze. Nello studio delle caratteristiche della fiamma sono state prese in considerazione le diverse diffusivit delle diverse specie chimiche costituenti la miscela. É stata sviluppata una nuova formulazione delle velocit di spostamento delle isosuperfici della variabile di progresso che tiene in conto delle diverse diffusivit delle specie chimiche.

1 Introduction

In many practical devices for power generation, such as stationary gas turbines, or propulsive systems, there has been a strong interest in achieving more efficiency and low polluttants emissions. For this purpose lean combustion burners are developed. The advantages of operating at lean mixture conditions are high thermal efficiency and low emissions of NO_x due to lower ame temperatures. Unfortunately at leaner conditions the flame tends to be thicker and propagate more slowly, suffering of flame instability. Local flame extinction occurs as a consequence of lean combustion conditions associated with stretching and heat losses. In order to overcome this issue, it possible increase the laminar burning velocity adding a small percentage of hydrogen to the lean premixed methane/air flame mixture. The hydrogen's large laminar burning velocity (approximately 7 times that of methane at 300 K and 1 bar) and the wider flammability limits allows the extension of the operational range of the combustion system. However, hydrogen is less energy dense than all other fuels, resulting in a loss of power in proportion to the base fuel substituted. For turbulent flames with hydrogen added to methane the literature is limited; we mention the experimental studies of [1, 4] and the two-dimensional DNS (with a chemical mechanism reduced to 19 species and 15 reactions) by Hawkes and Chen [5]. The topic of hydrogen addition has become important recently, in particular because of the need to increase the knowledge about the effects of biomass and coal gasication and addition of the obtained and shifted gases to regular fuels.

1.1 Problem configuration

The simulation was performed in a slot-burner Bunsen flame configuration. The slot-burner Bunsen configuration is especially interesting due to the presence of mean shear in the flow and is similar in configuration to the burner used in experimental studies [6]. This configuration consists of a central reactant jet through which premixed reactants are supplied. The central jet is surrounded on either side by a heated coflow, whose composition and temperature are those of the complete combustion products of the freely propagating jet mixture. The reactant jet was chosen to be a premixed methane/hydrogen air jet at 600 K and mixture equivalence ratio $\phi = 0.7$, with molar fractional distribution of 20% H_2 and 80% CH_4. The unstrained laminar flame properties at these conditions computed using Chemkin [16] are summarized in Table 1.1. In this table ϕ represents the multicomponent equivalence ratio of the reactant jet mixture, $\phi = [(X_{H_2} + X_{CH_4})/X_{O_2}]/[(X_{H_2} + X_{CH_4})/X_{O_2}]_{stoich}$, T_u is the unburned gas temperature, T_b the products gas temperature, s_L represents the unstrained laminar flame speed and $\delta_{th} = (T_b - T_u)/|\partial T/\partial x|_{max}$ is the thermal thickness based on maximum temperature gradient. Preheating the reactants leads to a higher flame speed and allows a higher inow velocity without blowing out the flame, reducing computational costs. Also, many practical devices such as gas turbines, internal combustion engines, and recirculating furnaces operate at highly preheated conditions. The simulation parameters are summarized in Table 1.2.

The domain size in the streamwise (z), crosswise (y) and spanwise (x) directions is $L_x \times L_y \times L_z = 24h \times 15h \times 2.5h$, h being the slot width ($h = 1.2$mm). The grid is uniform only in the x direction ($\Delta x = 20\mu$m), while is stretched in the y and z direction near the inlet duct walls. The DNS was run at atmospheric pressure

ϕ	$n_{H_2} = x_{H_2}/(x_{H_2} + x_{CH_4})$	T_u [K]	T_b [K]	s_L[cm s^{-1}]	δ_{th}[mm]
0.7	0.2	600	2072	103.75	0.3476

Tabella 1.1: CH_4/H_2 − Air laminar flame.

Slot width (h)	1.2 mm
Domain size in the spanwise (L_x), crosswise (L_y) and streamwise (L_z) directions	$24h \times 15h \times 2.5h$
$N_x \times N_y \times N_z$	$1550 \times 640 \times 140$
Turbulent jet velocity (U_0)	110 m s^{-1}
Coflow velocity	25 m s^{-1}
Jet Reynolds Number ($Re_{jet} = U_0 h/\upsilon$)	2264
Turbulent intensity (u'/S_L)	12.5
Turbulent length scale (l_t/δ_L)	2.6
Turbulent Reynolds Number ($Re_t = u'\eta_K/\upsilon$)	226
Damkohler number ($s_L L_t/u'L$)	0.21
Karlovitz number (δ_L/η_K)	503
Minimum grid space	9 μm
Kolmogorov Lenght Scale η_K	17.22 μm

Tabella 1.2: CH_4/H_2 – Air turbulent flame: the kinematic viscosity used in the calculation of Reynolds number is that of the inflow $CH_4 - H_2$/Air mixture $\nu = 5.3 \cdot 10^{-5}$ m^2 s^{-1}

using a 17 species and 73 elementary reactions kinetic mechanism [7]. The velocity of the central jet stream is 100 m/s, while the velocity of the coflow stream is 25 m/s. The width h of the central duct, where the inlet turbulent velocity profile may develop, is 1.2 mm and 4 mm long. The width walls of the duct h_w is 0.18 mm. Velocity fluctuations, $u' = 12$ m s^{-1}, are imposed on the mean inlet velocity profile, obtained by generating at duct's inlet homogeneous isotropic turbulence field with a characteristic turbulent correlation scale in the streamwise direction of $\delta_{corr} = 0.0004$ m and a streamwise velocity fluctuation of $u'_z = 12$ ms^{-1}, are imposed on the mean inlet duct's velocity profile by means of Klein's procedure [8]. The jet Reynolds number based on the centerline inlet velocity and slot width h is $Re_{jet} = Uh/\upsilon = 2264$. Based on the jet exit duct centerline velocity and the total streamwise domain lenght, the flow through time is $\tau_U = 0.218$ ms. Navier-Stokes characteristic boundary conditions (NSCBC) were adopted to prescribe boundary conditions. Periodic boundary conditions were applied in the x direction, while improved staggered non-reflecting inflow and outflow boundary conditions were fixed in y and z directions [9, 10]. The simulation was performed on the linux cluster CRESCO (Computational Center for Complex Systems) at ENEA, requiring 1.5 million CPU-hours running for 20 days on 3500 processors. The solution was advanced at a constant time step of 2.3 ns and after the flame reached statistical stationarity, the data were been collected through 4 τ_U.

1.2 Governing Equations

In LES each turbulent field variable is decomposed into a resolved and a subgrid-scale part. In this work, the spatial filtering operation is implicitly defined by the local grid cell size. Variables per unit volume are treated using Reynolds decomposition, while Favre (density weighted) decomposition is used to describe quantities per mass unit. The instantaneous small-scale fluctuations are removed by the filter, but their statistical effects remain inside the unclosed terms representing the influence of the subgrid scales on the resolved ones. In this article, a test deals with combustion to show the robustness of the suggested technique. Gaseous combustion is governed by a set of transport equations expressing the conservation of mass, momentum and energy, and by a thermodynamic equation of state describing the gas behaviour. For a mixture of N_s ideal gases in local thermodynamic equilibrium but chemical nonequilibrium, the corresponding filtered field equations (extended Navier−Stokes equations) are:

- Transport Equation of Mass

$$\frac{\partial \rho}{\partial t} + \frac{\partial \rho u_i}{\partial x_i} = 0. \tag{1.1}$$

- Transport Equation of Momentum

$$\frac{\partial (\rho u_j)}{\partial t} + \frac{\partial (\rho u_i u_j + p\delta_{ij})}{\partial x_i} = \frac{\partial \tau_{ij}}{\partial x_i} \tag{1.2}$$

- Transport Equation of Total Energy (internal + mechanical, $\mathcal{E} + \mathcal{K}$)

$$\frac{\partial (\rho \mathcal{U})}{\partial t} + \frac{\partial (\rho u_i \mathcal{U} + p u_i)}{\partial x_i} = -\frac{\partial (q_i - u_j \tau_{ij})}{\partial x_i} \tag{1.3}$$

- Transport Equation of the N_s Species Mass Fractions

$$\frac{\partial (\rho Y_n)}{\partial t} + \frac{\partial (\rho u_j Y_n)}{\partial x_i} = -\frac{\partial}{\partial x_i}(J_{n,i}) + \dot{\omega}_n \tag{1.4}$$

- Thermodynamic Equation of State

$$p = \rho \sum_{n=1}^{N_s} \frac{Y_n}{W_n} \mathcal{R}_u T \tag{1.5}$$

These equations must be coupled with the constitutive equations which describe the molecular transport. In the above equations, t is the time variable, ρ the density, u_j the velocities, τ_{ij} the viscous stress tensor, $\mathcal{U}$ the total filtered energy per unit of mass, that is the sum of the filtered internal energy, $\widetilde{e}$, and the resolved kinetic energy, $1/2\, u_i u_i$, q_i is the heat flux, p the pressure, T the temperature, $\mathcal{R}_u$ is the universal gas constant, W_n the nth-species molecular weight, $\dot{\omega}_n$ is the production/destruction rate of species n, diffusing at velocity $V_{i,n}$ and resulting in a diffusive mass flux $\boldsymbol{J_n} = \rho Y_n \boldsymbol{V_n}$. The stress tensor and the heat flux are respectively:

$$\tau_{ij} = 2\mu \left(S_{ij} - \frac{1}{3} S_{kk}\delta_{ij}\right) \tag{1.6}$$

$$q_i = -k\frac{\partial T}{\partial x_i} + \rho \sum_{n=1}^{N_s} h_n Y_n V_{i,n}. \tag{1.7}$$

In Eqn. 1.6-1.7 μ is the molecular viscosity and k is the termal conductivity.

The simulation were performed using the code HeaRT, which solves the fully compressible Navier-Stokes, species and total energy equations (1.1-1.4) with the fully explicit third-order accurate TVD Runge-Kutta scheme of Shu and Osher [21] and a sixth order compact staggered scheme for non-uniform grid (with the non uniform grid effects included in the compact coefficients scheme). No filter is necessary for ensuring stable solutions [22, 23, 24]. Fig. 1.1 shows the computational domain adopted in the simulation with a slice indicating the not uniform grid in the streamwise and crosswise directions (only one grid line each ten is represented), and the different stencils (due to the presence of walls and non periodic outlet) of the staggered compact scheme in the three coordinates directions.

1.2.1 Physical Properties and Kinetic Model

Kinetic theory is used to calculate dynamic viscosity and thermal conductivity of individual species [14]. The mixture-average properties are estimated by means of Wilke's formula with Bird's correction for viscosity [15],[16], and Mathur's expression for thermal conductivity [17].

Eqn. 1.7, the first term is the heat transfer by conduction, modeled by Fourier's law, the second is the heat transport due to molecular diffusion acting in multicomponent mixtures and driven by concentration gradients.

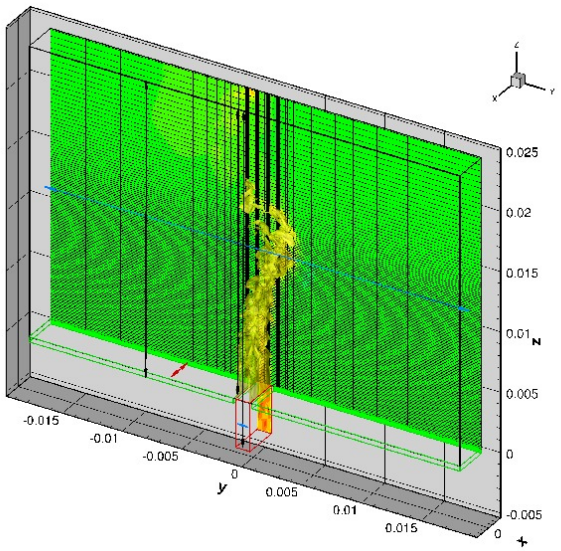

h!

Figura 1.1: Slice of instantaneous streamwise velocity with not uniform computational grid (for clarity only one grid line each ten is represented). Coloured arrows: the compact finite difference stencils in the three directions for each zone of the computational domain; Isosurface of temperature T = 700.

The Hirschfelder and Curtiss approximate formula for mass diffusion $\boldsymbol{V_n}$ in a multicomponent mixture and Soret effect are adopted, i.e.,

$$\begin{aligned} \boldsymbol{J_n} = \rho Y_n \boldsymbol{V_n} &= -\rho Y_n \sum_{i=1}^{N_s} D_{nj}^{\star} d_n - D_n^T \frac{\nabla T}{T} \\ &= -\rho \frac{W_n}{W_{mix}} D_n \nabla X_n - D_n^T \frac{\nabla T}{T} \ , \end{aligned} \tag{1.8}$$

with $X_n = Y_n W_{mix}/W_n$ and the D_n is

$$D_n = \frac{1 - Y_n}{\sum_{j=1,\ j\neq n}^{N_s} \frac{X_j}{\mathcal{D}_{jn}}} \ . \tag{1.9}$$

$\mathcal{D}_{jn}$ being the binary diffusion coefficient and D_n^T is the n-th species thermo diffusion coefficient and d_n the diffusional driving forces that for low-density gases became:

$$\boldsymbol{d_n} = \nabla X_n + (X_n - Y_n)\frac{\nabla p}{p}\frac{\rho}{p} \sum_{i=1, i\neq n}^{N_s} Y_i Y_n (\boldsymbol{f_i} - \boldsymbol{f_n}) \tag{1.10}$$

Only the first cross diffusion term of Eqn. 1.10 is retained in this work, while the pressure gradient diffusion (low subsonic flame flow) and the external forces diffusion (low-density gases assumption) are neglected.

Soret effect is due to the fact that for hard molecules, with interacting forces varying with distance more strongly than the inverse of the fifth power, there is a larger transfer of momentum in collisions with larger relative velocity of the colliding partners. For molecules of different masses, since the thermal agitation velocity of the i-th species is proportional to $(T/m_i)^{1/2}$, there will be more collisions with large relative velocity with lighter molecules coming from the hotter region and heavier coming from the colder than vice versa. The net transfer of momentum from heavy to light molecules is then directed towards the hotter part of the gas and the thermal diffusion ratio of light species is negative [19],[18]. Light molecules will have a tendency to stay in hot zone and leave cold zones and vice versa.

When inexact expressions for diffusion velocities are used (as when using Hirschfelder's law), and in general when differential diffusion effects are considered, the constrain $\sum_{i=1}^{N_s} \boldsymbol{J_i} = \sum_{i=1}^{N_s} \rho Y_i \boldsymbol{V_i} = 0$ is not necessarily satisfied. In this paper, to impose mass conservation, an artificial diffusion velocity $\boldsymbol{V^c}$ is subtracted from

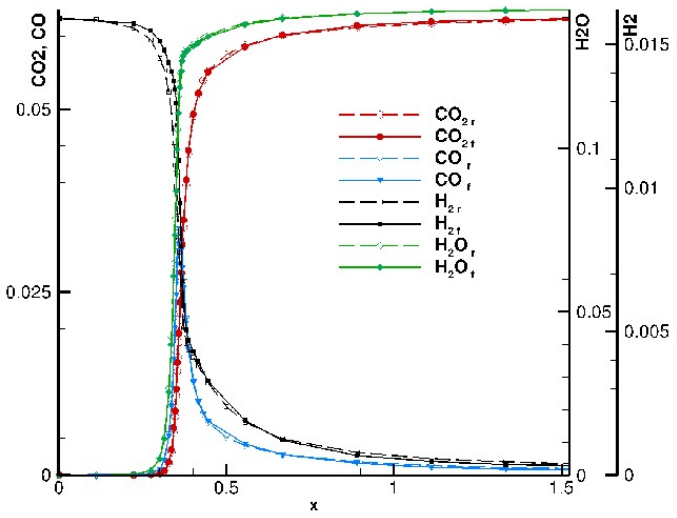

Figura 1.2: Comparison of species mole fraction in the detailed and reduced kinetic schemes: solid line) GRIMECH 3.0 kinetic scheme [11]; Long dashed line) Reduced kinetic scheme [7].

the flow velocity in the species transport equations [12]. This velocity, assuming Hirschfelder's law holds, becomes:

$$\boldsymbol{V^c} = -\sum_{n=1}^{N_s} \frac{W_n}{W_{mix}} D_n \nabla X_n \ . \tag{1.11}$$

Fig. 1.2-1.3 show freely propagating premixed ($\Phi = 0.7$) flame results obtained with the detailed (GRIMECH 3.0 [11]) and reduced kinetic scheme without the inclusion of the Soret effect (Eqn. 1.8) obtained by means of CHEMKIN code [16]. The thermochemical information on the gas phase and the Lennard Jones coefficients for the evaluation of transport properties were obtained primarily from the CHEMKIN database [16]. The maximum errors of the reduced scheme are $\sim 4\%$ and $\sim 6\%$ for the laminar flame velocity and temperature respectively.

Fig. 1.4 shows the gradient of temperature and the heat release in the normalized progress variable space c. The progress variable Y_c is defined as the sum of CO, CO_2, H_2O mass fractions while the :

$$c = \frac{Y_c - Y_{c,b}}{Y_{c,f} - Y_{c,b}} \tag{1.12}$$

where $Y_{c,f}$ and $Y_{c,b}$ are the proegress variable mass fractions in the fresh and burned gas respectively. The heat release is complete at $c \sim 0.9$. The maximum heat release is at c = 0.704, while the maximum value of temperature gradient, adopted for the calculation of laminar thermal thickness δ_{th}, is at c = 0.44.

Fig.1.5 shows the effects of preferential diffusion and Soret effect on the structure of the premixed laminar flames in the progress variable space. For the flame considered the only elements present are carbon, hydrogen, oxygen and nitrogen: m = C, H, O, N and the local equivalence ratio ϕ is calculated as:

$$\phi = \frac{2A_C + 0.5A_H}{A_O} \tag{1.13}$$

where $A_m = \sum_{k=1}^{K} \alpha_{k,m} x_k$ is the number of moles of atom of element m per mole of gas, $\alpha_{k,m}$ the number of atoms of element m per species k and x_k its mole fraction. Since chemical reactions do not change the elemental composition, and convection in an ideal one-dimensional system merely translates fluid without affecting its composition, variation of elemental composition with respect to distance in the freely propagating flame occurs as a result of axial differential diffusion of initial reactants, the major products and key intermediates such H.

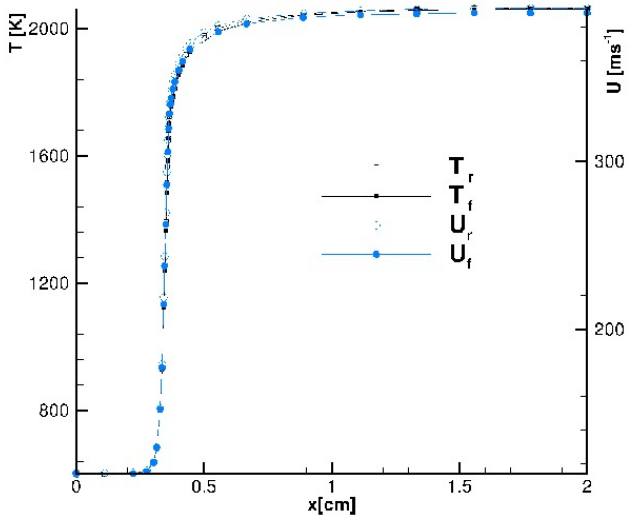

Figura 1.3: Comparison of velocity and temperature in the detailed and reduced kinetic schemes: solid line) GRIMECH 3.0 kinetic scheme [11]; Long dashed line) Reduced kinetic scheme [7].

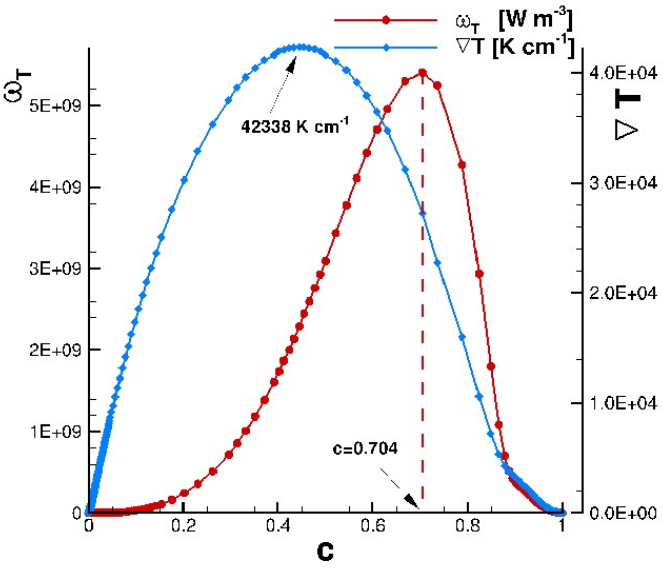

Figura 1.4: Temperature gradient (bullets) and heat reaction rate (squares) of unstretched premixed flame in progress variable space.

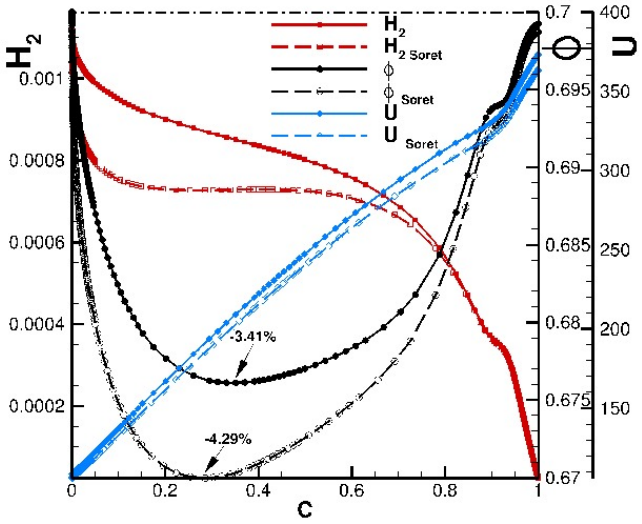

Figura 1.5: Laminar premixed flame solution in progress variable space: Solid lines) Without Soret effect included; LongDashed lines) With Soret effect included; Dot-Dashed line) Nominal inlet value equivalence ratio.

Calculated values of ϕ are shown in Fig.1.5, in the region of maximum temperature gradient the equivalence ratio decreases to $\phi \sim 0.675$ (the nominal inlet equivalence ratio $\phi = 0.7$ is indicated as an horizontal dot-dashed line).

Fig.1.5 shows also that the inclusion of the Soret effect in the laminar flame calculations decrease the local equivalence ratio and the flame velocity. In fact, since the thermal diffusion coefficients of molecular H_2, atomic hydrogen H and O, OH are negative, active radicals and deficient reactant are less prone to diffuse in the cold region and flame propagation velocity is lower ($\sim 3\%$). Although thermal diffusion as a single eect tends to drive H_2 towards the hot ame region, the nonlinear coupling between transport and chemistry results in the opposite effect, i.e., the H_2 concentration is actually lower in the hot ame region when thermal diffusion is included in the model. When the deficient reactant is more diffusive than heat (as in the case of H_2), any portion of a tridimensional premixed flame protruding into the fresh mixture (convex flame front) burn more vigorously because diffusive focusing of reactants into the flame is more rapid than heat diffusion away from the bulging front [25, 26]. Thermal diffusion (Soret effect) supplements the diffusive flux of fuel into the hot reaction zone, increasing the H_2 focusing effect and consequently the effective richness of the mixture in convex zones of the flame. These last two aspects will be quantified in the following sections.

2 Numerical Results

2.1 General characteristics of the flame

An overall description of the slot flame is given by the evolution, downstream the inlet channel, of the axial and radial velocities $\widetilde{U}_z$, $\widetilde{U}_y$ and their fluctuations shown in Fig. 2.1-2.3. The symbol $\widetilde{\phi}$ indicates Favre mean of the variable ϕ defined as $\widetilde{\phi}(y,z) = \overline{\rho\phi}/\overline{\rho}$, where ρ is the density and the overbar denotes ensemble averages defined as:

$$\overline{\phi}(y,z) = \frac{1}{N_d N_x} \sum_{n=1}^{N_d} \sum_{k=1}^{N_x} \phi(x_k, y, z, t_n). \tag{2.1}$$

with N_d is the number of data sets in a statistically stationary time period (approximately $\sim 8T_c = L_z/U_0$), N_d is the number of grid points in the x periodic direction. At the exit of the channel, the axial velocity U_z reach a maximum value of $110 ms^{-1}$ greater than its inlet value, due to formation of the channel boundary layer, that is equivant to a restriction of the flow section (see Fig.2.1).

Downstream, a crosswise component is generated in the coflow because of the presence of the central jet core (see streamlines in Fig.2.1 and U_y velocity profiles in Fig.2.2b). The blue lines indicates the flame brush thickness identified using a value of progress variable c between $(0.05 - 0.95)$. The Fig.2.1b shows the mean shear layer, defined as the velocity gradient in the crosswise direction, and the flame front location, identified with a value of $c = 0.7$ corresponding to the location of the maximum heat release of the unstrained laminar flame (see Fig. 1.4). Due to the presence of wall channel the maximum velocity gradient is located near the internal edges. The average flame front resides outside of the core of the jet near the wall duct and at 0.009mm moves towards the inside of the shear layer. The effect of the mixture jet expansion at the exit of channel and the coflow entrainement towards the jet core is evidenced in Fig. 2.2b (solid line). The velocity fluctuation is highest in the middle of the shear layer due to the mean shear of the jet and to the heat released by the flame, reach its maximum value at $z \sim 0.007$m and it decreases downstream. These variation of turbulent characteristics and the development of the flame downstream in the jet suggest that, in order to characterize the position of the flame in the premixed combustion regime diagram, the local turbulent lenght scale l_t, flame thickness δ_F and flame velocity S_L must be calculated. Here $l_t = u'^3/\tilde{\epsilon}$, with $\tilde{\epsilon}$ the average turbulent kinetic dissipation rate, $\delta_F = (\alpha\tau_{ch})^{1/2}$, and $S_L = (\alpha\tau_{ch})^{1/2}$, with $\tau_{ch} = \rho c_p T/|\sum_{n=1}^{N_s} H_n\omega_n|$.

Many modeling approaches, describe turbulent premixed flames as an ensemble of flame elements that resemble steadily propagating strained or curved laminar flames. When Karlovitz (Ka) number is between 1 and 100 small eddies can penetrate the diffusion preheating zone of the flame and increasing the mixing process, but not the thinner reaction layer that remains close to a wrinkled laminar reaction zone. This regime is identified as Thickened Reaction Zone (TRZ) regime. Fig.2.4, show the analysis that places the flame in the TRZ regime, results that will be confirmed later in the work, by analyzing some statistical properties of the flame.

2.2 Displacement speeds

Under the assumptions that a turbulent premixed flame retains locally the structure of a laminar flame but stretched and wrinkled by the serrounding turbulence, it is possible to separate the non linear nature of turbulence with that of the reaction rate defining a reaction progress variable, monotonically varying from 0 in the fresh reactants to 1. The flame zones are identified with progress variable isosurfaces, on which statistics are extracted. Once the species that define the normalized progress variable $c = (\sum_{i\in S} Y_i - \sum_{i\in S} Y_{i,u})/(\sum_{i\in S} Y_{i,b} - \sum_{i\in S} Y_{i,u})$,

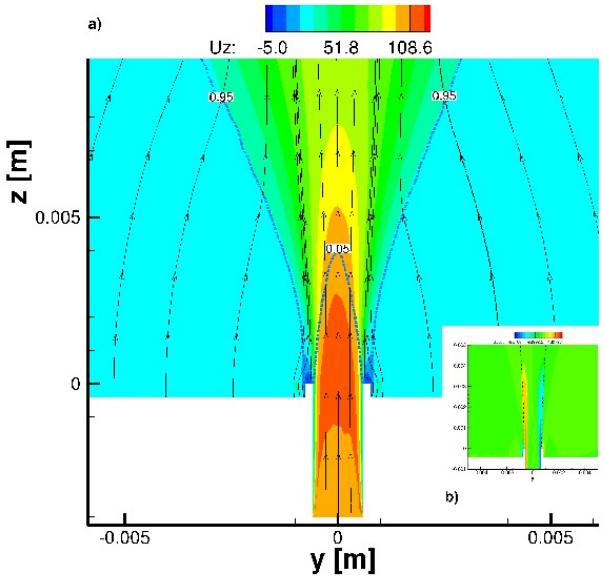

Figura 2.1: Mean streamwise velocity contour plot at the x = 0 plane. Also shown in the contour plot are the velocities streamlines and the iso-contour of $\widetilde{c} = 0.05 - 0.95$, indicating theh mean flame brush. b)The bottom right shows a zoomed in view of the velocity gradient $d\widetilde{U}_z/dy$ contour and the iso-contour of progress variable $\tilde{c} = 0.7$.

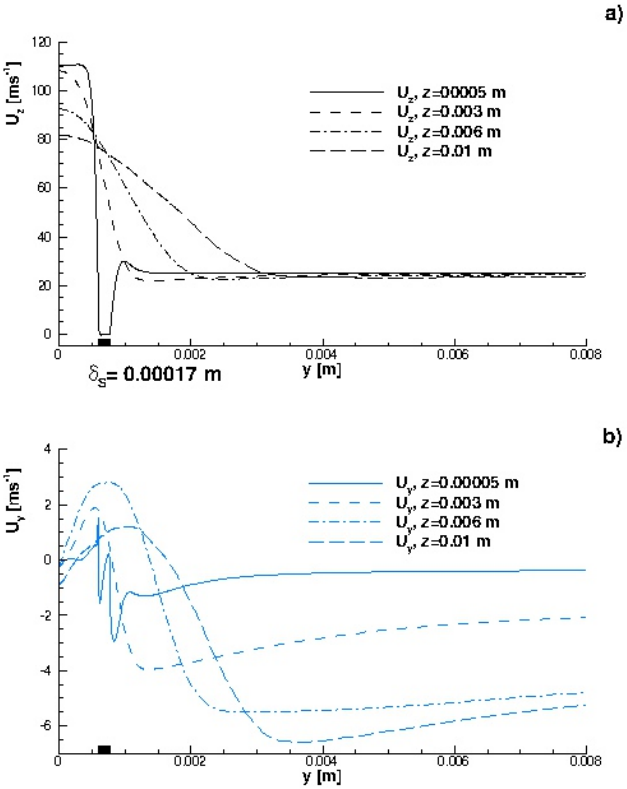

Figura 2.2: a) Mean streamwise velocity U_z versus crosswise direction y; b) Mean crosswise velocity U_y versus crosswise direction y.

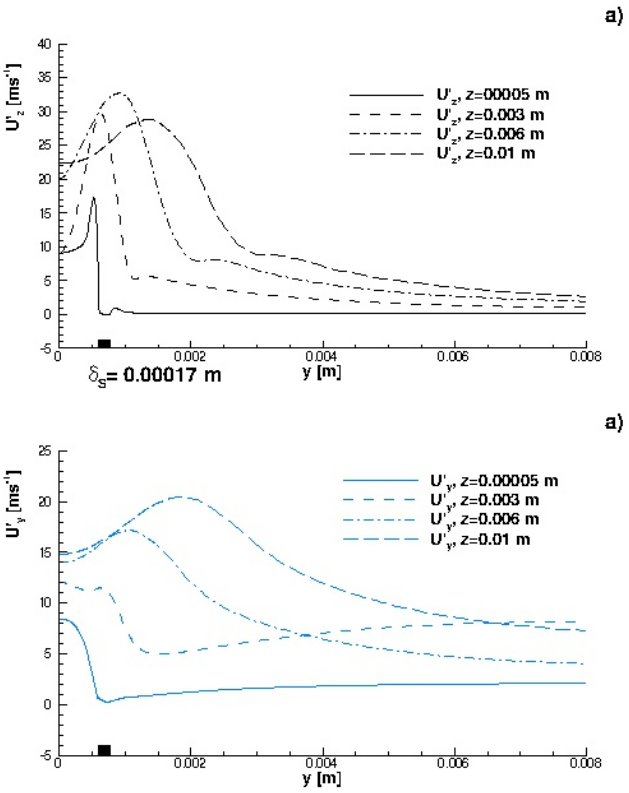

Figura 2.3: a) Mean streamwise rms-velocity U'_z versus crosswise direction y; b) Mean crosswise velocity U'_y versus crosswise direction y.

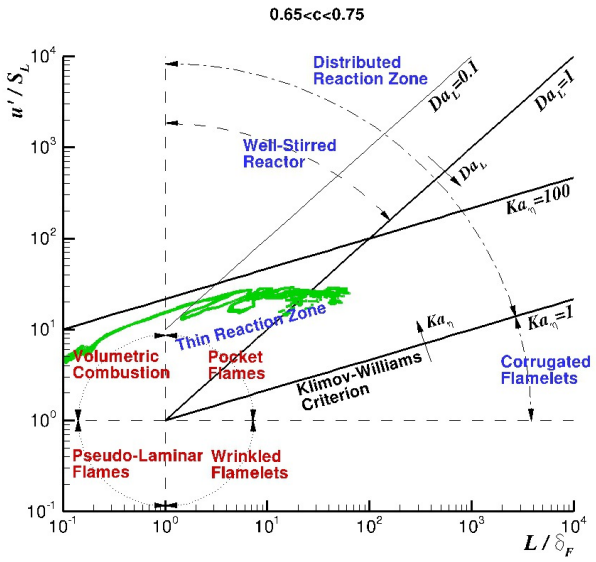

Figura 2.4: Borghi diagram.

are determined (in this case S={CO_2, CO, H_2O}), and considering that Differential Diffusion is taken into account and Hirschfelder and Curtiss formula for mass diffusion and Soret effect are included (Eqn.1.8), the classical governing transport equation must be revised as:

$$\frac{\partial c}{\partial t} + \boldsymbol{u} \cdot \nabla c = \frac{1}{\rho} \sum_{i \in S} \nabla \cdot (\rho \frac{W_i}{W_m} D_i \nabla X_i) + \frac{1}{\rho} \sum_{i \in S} \nabla \cdot (\frac{D_i^T}{T} \nabla T) + \frac{\dot{\omega}_c}{\rho} \tag{2.2}$$

with W_m the average mixture molecular weight. The mass diffusion term of Eqn. 2.2 based on the Hirschfelder and Curtiss formula may be split into a normal and tangential term recognizing that

$$\nabla X_i = \frac{W_m}{W_i} \nabla Y_i + \frac{Y_i}{W_i} \nabla W_m \tag{2.3}$$

with $\nabla Y_i = -|\nabla Y_i| \boldsymbol{n}$. Further expansion of the divergence operator, $\nabla \cdot ()$, yields for Eqn.2.2 to:

$$\begin{aligned} &\frac{\partial c}{\partial t} + \boldsymbol{u} \cdot \nabla c = \\ &\frac{1}{\rho Y_{c,Max}} \sum_{i \in S} (-\boldsymbol{n} \cdot \nabla (\rho D_i |\nabla Y_i|) - \rho D_i |\nabla Y_i| \nabla \cdot \boldsymbol{n} + \nabla \cdot (\frac{\rho D_i Y_i}{W_m} \nabla W_m)) + \\ &\frac{1}{\rho Y_{c,Max}} \sum_{i \in S} \nabla \cdot (\frac{D_i^T}{T} \nabla T) + \frac{\dot{\omega}_c}{\rho} \end{aligned} \tag{2.4}$$

Here, $\nabla \cdot \boldsymbol{n}$ is the curvature which may be expressed as the sum of the local inverses of the principal radii of curvature of the isosurface and flame surface curved convex towards the reactants is assumed to have positive curvature. The same equation can be written in kinematic form for a progress variable isosurface $c = c^*$ [27]:

$$[\frac{\partial c}{\partial t} + \boldsymbol{u} \cdot \nabla c]_{c=c^*} = S_d |\nabla|_{c=c^*} \tag{2.5}$$

where S_d, the displacement speed, is the magnitude of the propagation velocity of the isocontour with normal $\boldsymbol{n} = -(\nabla c / |\nabla c|)_{c=c^*}$ directed toward the unburnt gas. Considering Eqns. (2.2-2.5) the following expression for the displacement speed S_d is obtained:

$$\begin{aligned} S_d = [&\frac{1}{\rho |\nabla c| Y_{c,Max}} (\omega_c + \\ &\sum_{i \in S} (-\boldsymbol{n} \cdot \nabla (\rho D_i |\nabla Y_i|)) + \\ &\sum_{i \in S} (-\rho D_i |\nabla Y_i| \nabla \cdot \boldsymbol{n}) + \\ &\sum_{i \in S} (\nabla \cdot (\frac{\rho D_i Y_i}{W_m} \nabla W_m)) + \\ &\sum_{i \in S} \nabla \cdot (\frac{D_i^T}{T} \nabla T))]_{c=c^*}. \end{aligned} \tag{2.6}$$

This expression shows that $S_d = S_r + S_n + S_t + S_h + S_{td}$ is determined by the contributions of five contributions: (a) reaction of progress variable, (b) normal mass diffusion, c) tangential mass diffusion, d) a new term related to Hirschfelder and Curtiss formula for mass diffusion, e) thermal diffusion. The value of the displacement speed changes across the flame normal because of thermal expansion effects, using a density-weighted displacement speed $S_d^* = \rho S_d / \rho_u$ this effect may be largely reduced.

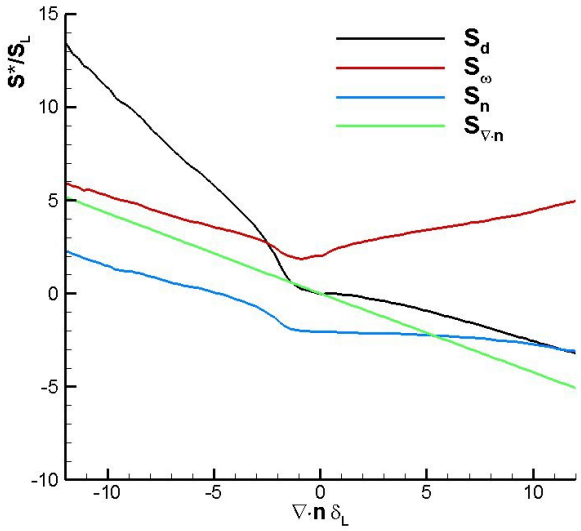

Figura 2.5: Density weighted mean displacement speed plotted against normalized curvature at c=0.7.

Figure 2.5 shows the density weighted mean (averaged on intervals of curvature) displacement speed and its components plotted against normalized curvature at isosurface c = 0.7. Curvature and flame displacement speed are negatively correlated and the flame is thermally stable. Flame elements with negative curvatures (curvature center in the unburnt mixture) propagate with faster flame speed than positively curved elements. Even though the local equivalence ratio decrease at negative curvature, due to preferential diffusion of H_2 towards hot regions, the effect of heat focusing at negative curvature increases the reaction rate of CH_4, as it has shown in Fig. 2.6, and consequently the isosurface displacement speed (that is related to reaction rate through S_r component).

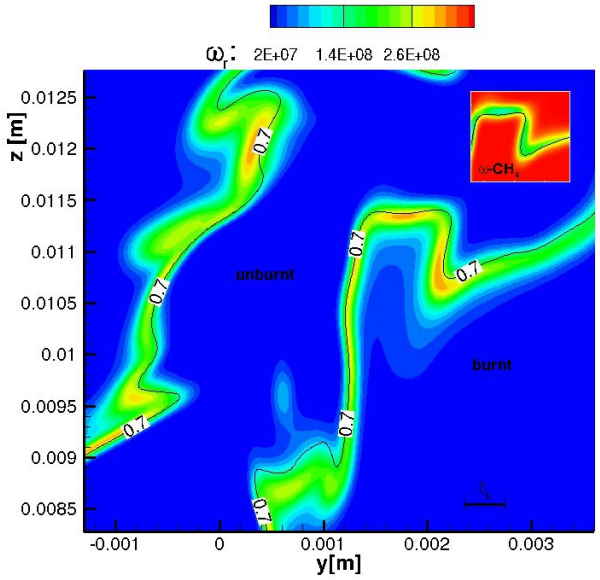

Figura 2.6: Instantaneous heat release [W m-3] contour map and zoomed in view of the CH4 reaction rate. The maximum of heat release is located at negative curvatures.

The local enrichment of the flame at positive curvature is shown also in Fig.2.7 where the instantaneous equivalence ratio, calculated with Eqn. 1.13, is shown. While in the laminar flame, the effect of the differential

diffusion is only a reduction towards leaner condition of the equivalence ratio, in the tridimensional DNS, the effect of positive curvature produces also local enrichment of the flame.

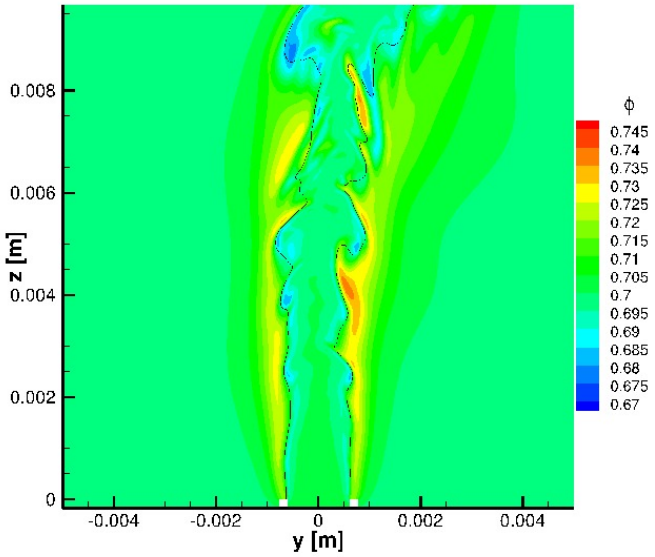

Figura 2.7: Instantaneous snapshot of the equivalence ratio ϕ calculated with Eqn.1.13 and isoline of progress variable c = 0.7.

In Fig. 2.5 it is evident that the flame is thermally stable, since the displacement speed of convex curvature regions is smaller than that of negative ones. Figure 2.8 shows the Probability Density Function (PDF) of the normalized density weighted mean displacement speed S_d^*/S_L and its components at c = 0.7. At c = 0.7, where the heat release is maximum, the total S_d is not symmetric around zero, with a skewness towards positive values of displacement speed and its peak is $S_s \sim 1ms^{-1}$.

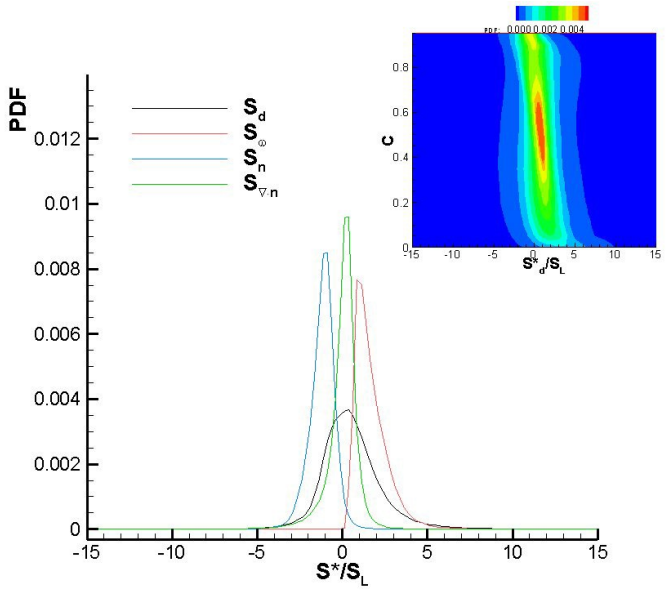

Figura 2.8: a) PDF of the density weighted mean displacement speed S_d^*/S_L and its three components at c=0.7; b) PDF of S_d^*/S_L as a function of c.

In the pre-heating zone of the flame (c < 0.5) the PDF presents a broader range of velocities, thus implying

non parallel iso-c surfaces in agreement with the Thin Reaction Regime, where small eddies may affect the pre-heating zone more than the reaction layer.

2.3 Flame thickness and curvature

In this section the effect of turbulence on flame stirring is studied. The magnitude of the progress variable,$|\nabla c|$ is adopted here as a measure of the flame thickness. Figure 2.9 shows the conditional mean of normalized $|\nabla c|$ (the laminar flame thickness δ_L is used as normalizing factor).

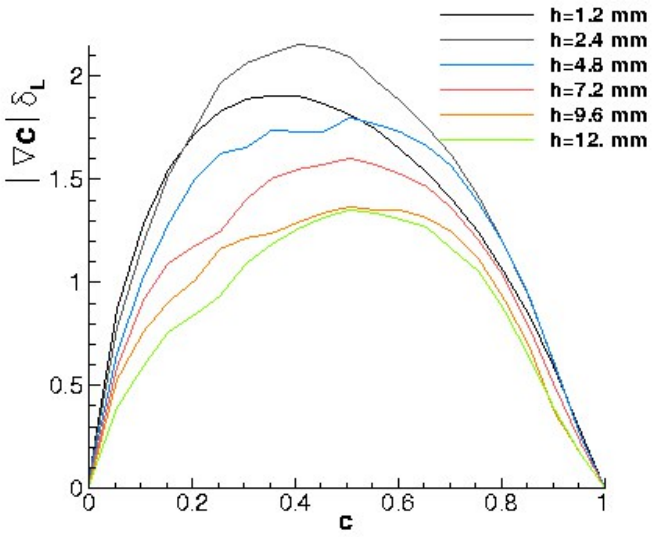

Figura 2.9: Conditional means of $|\nabla c|$ versus progress variable at different heights in the turbulent flame.

The results show that the flame thickness calculated as the inverse of the magnitude of the gradient of progress variable $\sim 1/|\nabla c|$ is lower than the laminar flame thickness δ_L. It decreases up to an height of 2.4mm in the flame and then it increases downstream. This is due to the development of the shear layer near the exit of the mixture channel and to the local increase of the strain rate that reduce the thickness of the flame. Going downstream the gradient of the velocities in the crosswise direction decreases and the flame thickness increases. The flame thickening found in this study is in agreement with some experimental results [28].

Figure 2.10 shows mean normalized curvature at different heights in the flame and c = 0.7. The distribution of curvatures is not symmetric about zero, it has longer tail for positive curvature and its maximum shifts towards negative curvature moving downstream from the injection channel.

Figure 2.11 shows the PDF of normalized curvature as a function of the progress variable. It is seen that the distribution of curvature has a negative peak value in the reaction zone (c > 0.5) while this peaks tend to reach positive values in the diffusion layer (c < 0.5).

2.4 Conclusions

A 3D slot $CH_4 - H_2/Air$ flame was simulated with a high-order compact staggered numerical scheme and detailed chemical mechanism. Displacement speeds as function of curvature are examined. Preferential diffusion of H_2 into positively curved flame elements are evidenced, the effect of mass differential diffusion calculated with the Hirschfelder formula was included in the displacement speed and a new expression was found for the displacement speed in the case of differential diffusion for the species. The lean flame is intrinsically stable as shown by the displacement speed as a function of the curvatures, since negative curvature flame elements present higher velocity than positive ones. Further work is necessary to understand quantitative effect of H_2 on structure of the flame. The simulation of the same flame with the Soret effect included in the transport equations

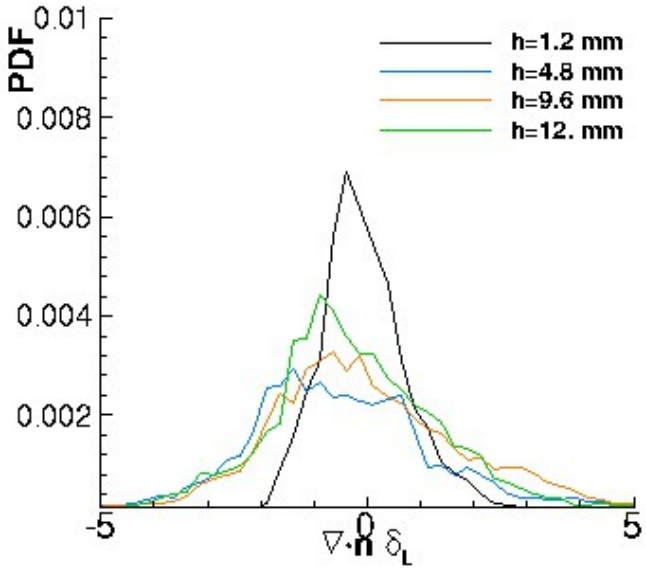

Figura 2.10: Probability density function of normalized curvature at different heights in the turbulent flame.

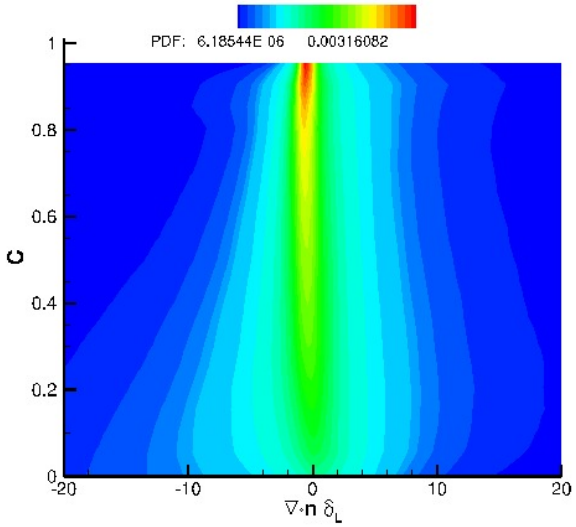

Figura 2.11: Probability density function of normalized curvature in function of the progress variable c in the turbulent flame.

is actually running on the CRESCO supercomputer cluster. The analysis done for the flame must be repeated for these results in order to quantify the role of thermal diffusion on statistics and stability of the flame.

Bibliografia

[1] R.W. Schefer, D.M. Wicksall, A.J. Agrawal, Combustion of hydrogen-enriched methane in a lean premixed swirl stabilized burner. Proc. Comb. Inst. 2003;29:843-51.

[2] F. Cozzi, A. Coghe, Behavior of hydrogen-enriched non-premixed swirled natural gas flames. Int J. Hydrogen Energy 2006;31:669-77.

[3] C. Mandilas, M.P. Ormsby, C.G.W. Sheppard, R. Woolley, Effects of hydrogen addition on laminar and turbulent premixed methane and iso-octaneair flames, Proc. Combust. Inst. 2007;31:1443-50.

[4] F. Halter, C. Chauveau, I. Gokalp, Characterization of the effects of hydrogen addition in premixed methane/air flames. Int J Hydrogen Energy 2007;32:2585-92.

[5] E.R. Hawkes, J.H. Chen, Direct numerical simulation of hydrogen-enriched lean premixed Methane-Air Flames, Combust. Flame 138 (2004) 242-58.

[6] S.A. Filatyev, J.F. Driscoll, C.D. Carter, J.M. Donbar, Measured properties of turbulent premixed Flames for model assessment, including burning velocities, stretch rates, and surface densities, Combust. Flame 141, 1-21, 2005.

[7] R. Sankaran, E.R. Hawkes, J.H. Chen, T. Lu, C.K. Law, Structure of a spatially developing turbulent lean methane-air Bunsen flame, Proc. Combust. Inst., 31, (2007) 1291-1298.

[8] M. Klein, A. Sadiki, J. Janicka, A digital filter based generation of inflow data for spatially developing direct numerical or large eddy simulations, J. Comput. Phys. 186, (2003), 652-665.

[9] T.J. Poinsot, S.K. Lele: Boundary Conditions for Direct Simulations of Compressible Viscous Flow. J. Comput. Phys., 101:104-129 (1992).

[10] J.C. Sutherland , C.A. Kennedy , Improved boundary conditions for viscous, reacting, compressible Flows, J. Comput. Phys., 191:502-524, 2003

[11] G.P. Smith, D.M. Golden, M. Frenklach, N.W. Moriarty, B. Eiteneer, M. Goldenberg, C.T. Bowman, R.K. Hanson, S. Song, W.C. Gardiner, V.V. Lissianski, Z. Qin, , `http://www.reactionengines.co.uk/news_updates.html`.

[12] T. Poinsot, D. Vaynante, Theoretical and numerical combustion, 2012.

[13] E. Giacomazzi, V. Battaglia and C. Bruno, The Coupling of Turbulence and Chemistry in a Premixed Bluff-Body Flame as Studied by LES, Combust. Flame, 138 (2004) 320-335.

[14] R.B. Bird, W.E. Stewart, E.N. Lightfoot, Transport Phenomena, Wiley International Edition, (2002).

[15] C.R. Wilke, J. Chem. Phys., 18, (1950), 517-9.

[16] R.J. Kee, G. Dixon-Lewis, J. Warnatz, M.E. Coltrin, Miller JA, Moffat HK, The CHEMKIN Collection III: Transport, San Diego, Reaction Design, (1998).

[17] S. Mathur, P.K. Tondon, S.C.Saxena, Molecular Physics, 12:569, (1967).

[18] J.H. Ferziger, H.G. Kaper, Mathematical Theory of Transport Processes in Gases, North Holland Pub. Co., Amsterdam, 1972.

[19] W.H. Furry, Am. J. Phys. 16 (1948) 63-78.

[20] E. Giacomazzi, F.R. Picchia, N.M. Arcidiacono, A Review on Chemical Diffusion, Criticism and Limits of Simplified Methods for Diffusion Coefficients Calculation, Combust. Theory Model., (2008).

[21] C.W. Shu, S. Osher, Efficient implementation of essentially non-oscillatory shock-capturing schemes, J. Comput. Phys., 77, 439-471 (1988).

[22] S.K. Lele, Compact finite difference schemes with spectral like resolution, J. Comput. Phys., 103, 16-42, (1992).

[23] S. Nagarajan, S.K. Lele, J.H. Ferziger, A robust high order compact method for large eddy simulation, J. Comput. Phys., 191, 392, 2003.

[24] L. Gamet, F. Ducros, F. Nicoud, T. Poinsot, Compact finite difference scheme on non-uniform meshes. Application to direct numerical simulations of compressible flows, Int. J. Numer. Meth. Fluids, 29,159-191, (1999).

[25] G.I. Sivashinsky, Anuu. Rev. Fluid Mech. 15, (1983) 179-200.

[26] Y.B. Zeldovich, Theory of Combustion and Detonation in Gases, Acad. Sci. USSR, (1944).

[27] T. Echekki, J.H. Chen, Unsteady strain rate and curvature effect in turbulent premixed methane-air flames, Combust. Flame, 106, (1996), 184.

[28] M.S. Mansour, N. Peters, Y.C. Chen, Proc. Combust. Inst. 27 (1998) 767-773.